

A probabilistic multi-object deformable model for MR/SPECT brain image registration and segmentation

Christophoros NIKOU^{†,‡}

Fabrice HEITZ[†]

Jean-Paul ARMSPACH[‡]

[†]Laboratoire des Sciences de l'Image, de l'Informatique
et de la Télédétection, CNRS UPRES-A 7005
University of Strasbourg I
4 Bd. Sébastien Brant, 67400 Illkirch, France

[‡]Institut de Physique Biologique, CNRS UPRES-A 7004,
University of Strasbourg I, Faculté de Médecine
4 rue Kirschleger, 67085 Strasbourg, France

ABSTRACT

A probabilistic deformable model for the representation of brain structures is described. The statistically learned deformable model represents the relative location of head (skull and scalp) and brain surfaces in MR/SPECT images pairs and accommodates the significant variability of these anatomical structures across different individuals. To provide a training set, a representative collection of 3D MRI volumes of different patients have first been registered to a reference image. The head and brain surfaces of each volume are parameterized by the amplitudes of the vibration modes of a deformable spherical mesh. For a given MR image in the training set, a vector containing the largest vibration modes describing the head and the brain is created. This random vector is statistically constrained by retaining the most significant variation modes of its Karhunen-Loeve expansion on the training population. By these means, both head and brain surfaces are deformed according to the anatomical variability observed in the training set. Two applications of the probabilistic deformable model are presented: the deformable model-based registration of 3D multimodal (MR/SPECT) brain images and the segmentation of the brain from MRI using the probabilistic constraints embedded in the deformable model. The multi-object deformable model may be considered as a first step towards the development of a general purpose probabilistic anatomical atlas of the brain.

Keywords: Physics-based deformations, Karhunen-Loeve decomposition, stochastic and deterministic optimization, image registration, image segmentation, Magnetic Resonance Imaging (MRI), Single Photon Emission Computed Tomography (SPECT).

1. INTRODUCTION

Since the seminal work of Kass *et al.*¹ on 2D shape models, deformable models have gained increasing popularity in computer vision to segment, match or track rigid and nonrigid objects.²⁻⁷ In medical image analysis, deformable models offer a unique and powerful approach to accommodate the significant variability of biological structures over time and across different individuals. A survey on deformable models as a promising computer-assisted medical image analysis technique has been presented by McInerney and Terzopoulos.⁸ Applications in medical image analysis include the segmentation of anatomical structures and the registration of multiple images.

Among the different segmentation methods, *deformable model-based segmentation* relies on or deformable models of the anatomical structures of interest. Statistical deformable models,^{2,3,9} in particular, are good candidate for representing the statistical variability of anatomical structures. For instance, a multislice 2D point distribution model (PDM)² has been deformed to match various structures in single modal PET images.¹⁰ 3D physically-based

Other author information:

Send correspondence to C.N. LSIIT-GRI, 4 boulevard Sbastien Brant, 67400 Illkirch, France

C.N.: Email: nikou@mondrian.u-strasbg.fr; Telephone: ++ 33 3 88 65 50 51; Fax ++ 33 3 88 65 52 49

F.H. Email: Fabrice.Heitz@ensps.u-strasbg.fr; Telephone: ++ 33 3 88 65 50 35; Fax: ++ 33 3 88 65 52 49

J.P.A. Email: armspach@alsace.u-strasbg.fr; Telephone: ++ 33 3 88 14 48 44; Fax: ++ 33 3 88 37 14 97

deformable models^{11–13} constrained by statistical analysis^{4,14} have also been applied to characterize pathological shape deformations.^{15,16}

A large variety of medical image registration methods has also been proposed in the literature.^{17,18} Among them, *deformable model-based registration methods* use extracted or modeled anatomical structures (usually curves or surfaces) to guide the matching process. The majority of these methods are concerned with non-rigid, intra-modality, and inter-subject registrations. They are based on mathematical models carrying *a priori* knowledge (atlases), that are deformed to match an image (model to modality registration)^{19,10,20,21} or on the elastic deformation of the entire volume of a subject image to match another subject data (intra-modality inter-subject registration) under some mathematical constraints.^{5,22–24}

The approach proposed here relies on a 3D physical deformable model that embeds information on the structures that may be extracted from different image modalities. The different model parts are statistically constrained to represent the structures of interest and their spatial relations in the different image modalities. These constraints are learned from a representative population in an off-line training procedure. The head (skull and scalp) and brain surfaces are extracted from a training set of 3D MRI. These surfaces are then parameterized by the amplitudes of the vibration modes of a physically-based deformable model⁴ and a joint model is constructed for each head/brain pair. The joint model is then statistically constrained by a Karhunen-Loeve decomposition. By these means, the spatial relation between head and brain structures, as well as, the anatomical variability observed in the training set are compactly described by a limited number of parameters.

Two applications of the probabilistic deformable model are presented:

- The deformable model-based registration of 3D multimodal (MR/SPECT) brain images by optimizing an energy function relying on the distance between the statistically constrained model parts and noisy multimodal data.
- The segmentation of the brain from MRI using the probabilistic constraints embedded in the deformable model. Given a MRI volume, the head is easily segmented by simple thresholding and region growing techniques. The deformable model parameters that match the segmented head surface are next recovered by solving an overconstrained linear system. The deformable model is then used to predict the brain surface in the same image. This first, approximate, but generally already accurate segmentation, is finally refined using iterative deterministic optimization.

The remainder of this paper is organized as follows : in Section 2, the parameterization of the head and brain structures by the vibration modes of a spherical mesh is presented. The statistical training procedure is described in Section 3. The application of the probabilistic model to multimodal image registration is presented in Section 4. Brain segmentation from MRI is described in Section 5. Finally, discussion and conclusion are presented in Section 6

2. A MULTI-OBJECT PHYSICS-BASED DEFORMABLE MODEL

To provide a training set, a representative collection of 3D MRI volumes of different patients have first been registered to a reference image using an unsupervised robust registration technique developed by the authors.^{25,26} The head of each volume has then been segmented by simple thresholding²⁷ and region growing. The brain has also been segmented by a semi-manual technique consisting of thresholding and region growing.²⁸ Both head and brain contours have been parameterized by the amplitudes of the vibration modes of a deformable spherical mesh.⁴

The model consists of 3D points sampled on a spherical surface, following a quadrilateral cylinder topology in order to avoid singularities due to the poles. Each node has a mass m and is connected to its four neighbours with springs of stiffness k . The model nodes are stacked in vector:

$$\mathbf{X} = (x_1, y_1, z_1, \dots, x_N, y_N, z_N, \dots, x_{2N}, y_{2N}, z_{2N}, \dots, x_{N'N}, y_{N'N}, z_{N'N})^T \quad (1)$$

where N is the number of points in the direction $0 \leq \phi \leq 2\pi$ and N' is the number of points in the direction $0 \leq \theta \leq \pi$. The model is also characterized by its mass matrix \mathbf{M} , its stiffness matrix \mathbf{K} and its evolution over time is controled by its dumping matrix \mathbf{C} . The system evolution equation is :

$$\mathbf{M}\ddot{\mathbf{U}}(t) + \mathbf{C}\dot{\mathbf{U}}(t) + \mathbf{K}\mathbf{U}(t) = \mathbf{F}(t) \quad (2)$$

where

$$\mathbf{U} = [\vec{\mathbf{U}}_1^T(t), \dots, \vec{\mathbf{U}}_N^T(t), \dots, \vec{\mathbf{U}}_{2N}^T(t), \dots, \vec{\mathbf{U}}_{N'N}^T(t)]^T \quad (3)$$

stands for the nodal displacements. Vector $\vec{\mathbf{U}}_i^T(t)$ represents the displacement of node i with respect to the x , y and z axes.

The image force vector $\mathbf{F}(t)$ is constructed as following: at first, a scalar $\mathbf{g}_i(t)$ corresponding to the chamfer distance between node i and its nearest contour point is computed²⁹ (fig. 1). The gradient $\nabla \mathbf{g}_i(t)$ of the above

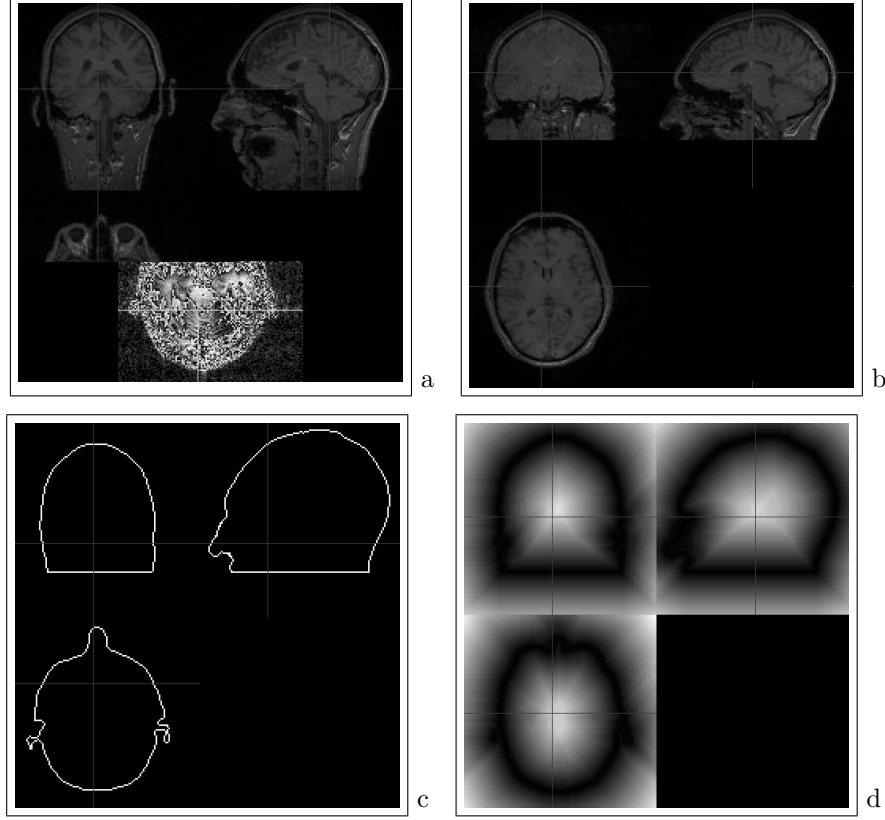


Figure 1. (a) A MR image of the training set. (b) Image in (a) segmented from its background. (c) Binary contour of image in (b). (d) Chamfer distance transform of image in (c).

potential with respect to the three Euclidean space directions provides the following force vectors:

$$\mathbf{G}(t) = [\nabla \mathbf{g}_1^T(t), \dots, \nabla \mathbf{g}_N^T(t), \dots, \nabla \mathbf{g}_{2N}^T(t), \dots, \nabla \mathbf{g}_{N'N}^T(t)]^T \quad (4)$$

In order to catch fine details of the object surface, the force \mathbf{G} is projected onto the vector normal to the surface at each model node. By these means, each point of the spherical mesh evolves along its normal direction and the amplitude of the displacement is determined by the projection of the image force onto this normal vector :

$$\mathbf{F}(t) = \langle \mathbf{G}(t), \vec{\mathcal{N}} \rangle \vec{\mathcal{N}} \quad (5)$$

where

$$\mathcal{N}(t) = [\vec{\mathcal{N}}_1^T(t), \dots, \vec{\mathcal{N}}_N^T(t), \dots, \vec{\mathcal{N}}_{2N}^T(t), \dots, \vec{\mathcal{N}}_{N'N}^T(t)]^T \quad (6)$$

$\vec{\mathcal{N}}_i^T(t)$ designates the normal to the surface vector at node i and $\langle \cdot, \cdot \rangle$ stands for the dot product.

Change of basis

Since equation (2) is of order $3NN'$, where NN' is the total number of nodes of the spherical mesh, it is solved in a subspace corresponding to the truncated vibration modes⁴ using the following change of basis:

$$\mathbf{U} = \mathbf{\Phi}\tilde{\mathbf{U}} = \sum_i \tilde{u}_i \phi_i, \quad (7)$$

where $\mathbf{\Phi}$ is a matrix and $\tilde{\mathbf{U}}$ is a vector, ϕ_i is the i^{th} row of $\mathbf{\Phi}$ and \tilde{u}_i is a scalar. By choosing $\mathbf{\Phi}$ as the matrix whose columns are the eigenvectors of the eigenproblem:

$$\mathbf{K}\phi_i = \omega_i^2 \mathbf{M}\phi_i, \quad (8)$$

\mathbf{M} and \mathbf{K} are simultaneously diagonalized and the system (2) is simplified to $3NN'$ scalar equations⁴:

$$\ddot{\tilde{u}}_i(t) + \tilde{c}_i \dot{\tilde{u}}_i(t) + \omega_i^2 \tilde{u}_i(t) = \tilde{f}_i(t). \quad (9)$$

In equation (9), ω_i designates the i^{th} eigenvalue, \tilde{u}_i is the amplitude of the corresponding vibration mode, \tilde{c}_i are the nonzero (diagonal) elements of

$$\tilde{\mathbf{C}} = \mathbf{\Phi}^T \mathbf{C} \mathbf{\Phi} \quad (10)$$

and

$$\tilde{f}_i(t) = \mathbf{\Phi}^T [(\mathbf{F}(t), \vec{\mathcal{N}}) \vec{\mathcal{N}}]. \quad (11)$$

The nondiagonal elements of $\tilde{\mathbf{C}}$ are zero because we have simplified the dumping matrix of the system by assuming that the dumping matrix \mathbf{C} is constructed using the Caughey series³⁰:

$$\mathbf{C} = \mathbf{M} \sum_{k=0}^{p-1} \alpha_k [\mathbf{M}^{-1} \mathbf{K}]^k \quad (12)$$

For $k = 2$, equation (12) reduces to Rayleigh dumping¹¹:

$$\mathbf{C} = \alpha_0 \mathbf{M} + \alpha_1 \mathbf{K} \quad (13)$$

and equation (10) provides us with the diagonal matrix:

$$\tilde{\mathbf{C}} = \alpha \mathbf{I} + \beta \mathbf{\Omega} \quad (14)$$

where \mathbf{I} is the identity matrix and $\mathbf{\Omega}$ is the diagonal matrix whose elements are the eigenvalues ω_i .

In our application, the deformable spherical mesh has a cylinder topology in order to avoid singularities due to the two poles. Let us also notice that the eigenvectors and the eigenvalues of a quadrilateral mesh with cylinder topology have an explicit expression. The eigenvalues are given by the equation:

$$\omega_{p,p'}^2 = \frac{4k}{m} \left(\sin^2 \frac{p\pi}{2N} + \sin^2 \frac{p'\pi}{N'} \right) \quad (15)$$

and the eigenvectors are obtained by:

$$\phi_{p,p'} = \left[\dots, \cos \frac{(2n-1)p\pi}{2N} \cos \frac{2n'p'\pi}{N'}, \dots \right]^T \quad (16)$$

with $n \in \{1, 2, \dots, N\}$ et $n' \in \{1, 2, \dots, N'\}$. For a cylinder topology:

$$\begin{cases} p & \in \{0, \dots, N-1\} & , \\ p' & \in \{-\frac{N'}{2} + 1, \dots, \frac{N'}{2}\} & , \quad N' \text{ even} \\ p' & \in \{-\frac{N'-1}{2}, \dots, \frac{N'-1}{2}\} & , \quad N' \text{ odd} \end{cases}$$

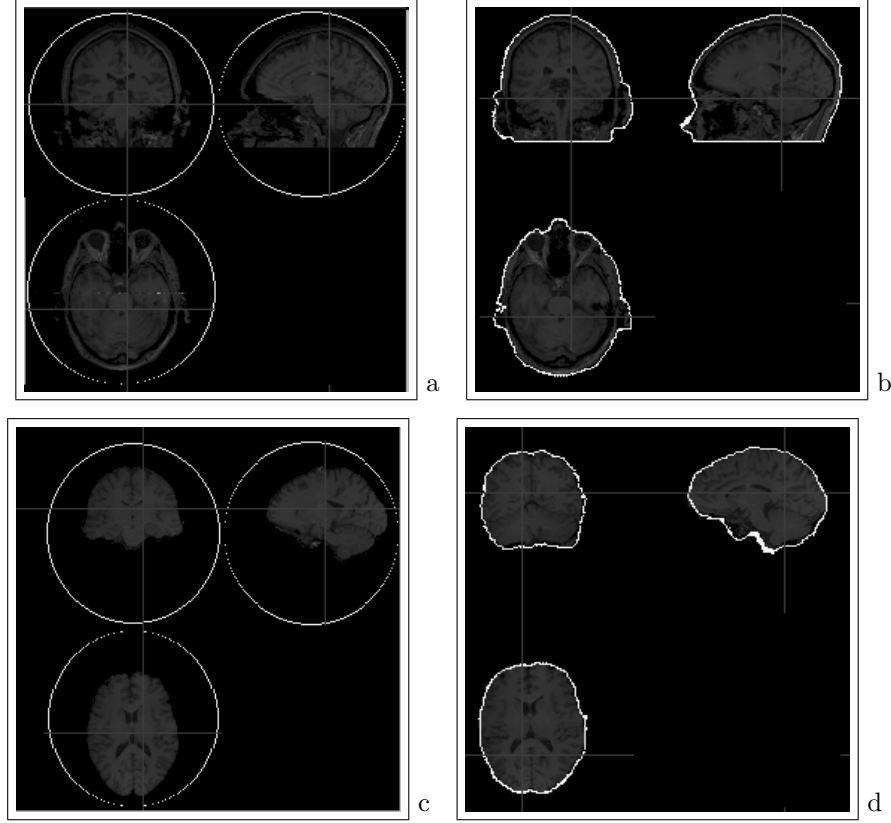


Figure 2. Head and brain parameterization from 3D MRI. (a) A head image and the initial spherical mesh superimposed. (b) The deformable model at equilibrium. (c) The segmented brain from the image in (a) and the initial spherical mesh superimposed. (d) The deformable model at equilibrium.

3. STATISTICAL TRAINING

For each image pair $i = 1, \dots, n$ in the training set, a vector \mathbf{a}_i containing the M' lowest frequency vibration modes describing the head ($\tilde{\mathbf{u}}_i^h$) and the M'' lowest frequency vibration modes describing the brain ($\tilde{\mathbf{u}}_i^b$) is then created:

$$\mathbf{a}_i = (\tilde{\mathbf{u}}_i^h, \tilde{\mathbf{u}}_i^b)^T \quad (17)$$

where:

$$\tilde{\mathbf{u}}_i^h = (\tilde{u}_1^h, \tilde{u}_2^h, \dots, \tilde{u}_{M'}^h)_i \quad (18)$$

$$\tilde{\mathbf{u}}_i^b = (\tilde{u}_1^b, \tilde{u}_2^b, \dots, \tilde{u}_{M''}^b)_i \quad (19)$$

with $3(M' + M'') < 6NN'$.

Random vector \mathbf{a} is statistically constrained by retaining the most significant variation modes in its Karhunen-Loeve (KL) transform^{2,3,14}:

$$\mathbf{a} = \bar{\mathbf{a}} + \mathbf{P}\mathbf{b} \quad (20)$$

where

$$\bar{\mathbf{a}} = \frac{1}{n} \sum_{i=1}^n \mathbf{a}_i \quad (21)$$

is the average vector of vibration amplitudes of the structures belonging to the training set, \mathbf{P} is the matrix whose columns are the eigenvectors of the covariance matrix

$$\mathbf{\Gamma} = \mathbb{E}[(\mathbf{a} - \bar{\mathbf{a}})^T(\mathbf{a} - \bar{\mathbf{a}})] \quad (22)$$

and

$$\mathbf{b}_i = \mathbf{P}^T(\mathbf{a}_i - \bar{\mathbf{a}}) \quad (23)$$

are the coordinates of $(\mathbf{a} - \bar{\mathbf{a}})$ in the eigenvector basis.

The deformable model (corresponding to the head and brain contours) is finally parameterized by the m most significant statistical deformation modes stacked in vector \mathbf{b} . By modifying \mathbf{b} , both the head and the brain are deformed (fig. 3), according to the anatomical variability observed in the training set. Given the double initial spherical mesh:

$$\bar{\mathbf{X}} = \begin{pmatrix} \bar{\mathbf{X}}_H \\ \bar{\mathbf{X}}_B \end{pmatrix} \quad (24)$$

where

$$\bar{\mathbf{X}}_H = (\bar{x}_1^h, \bar{y}_1^h, \bar{z}_1^h, \dots, \bar{x}_{N'N'}^h, \bar{y}_{N'N'}^h, \bar{z}_{N'N'}^h)^T \quad (25)$$

$$\bar{\mathbf{X}}_B = (\bar{x}_1^b, \bar{y}_1^b, \bar{z}_1^b, \dots, \bar{x}_{N'N'}^b, \bar{y}_{N'N'}^b, \bar{z}_{N'N'}^b)^T \quad (26)$$

the deformable multimodel $\mathbf{X}(\mathbf{b})$ is thus represented by:

$$\mathbf{X}(\mathbf{a}) = \bar{\mathbf{X}} + \Phi \mathbf{a} \quad (27)$$

Combining equations (20) and (27) we have:

$$\mathbf{X}(\mathbf{b}) = \bar{\mathbf{X}} + \Phi \bar{\mathbf{a}} + \Phi \mathbf{P} \mathbf{b} \quad (28)$$

where

$$\Phi = \begin{pmatrix} \Phi_H & \mathbf{0} \\ \mathbf{0} & \Phi_B \end{pmatrix}, \quad \mathbf{P} = \begin{pmatrix} \mathbf{P}_{HB} \\ \mathbf{P}_{BH} \end{pmatrix} \quad (29)$$

and

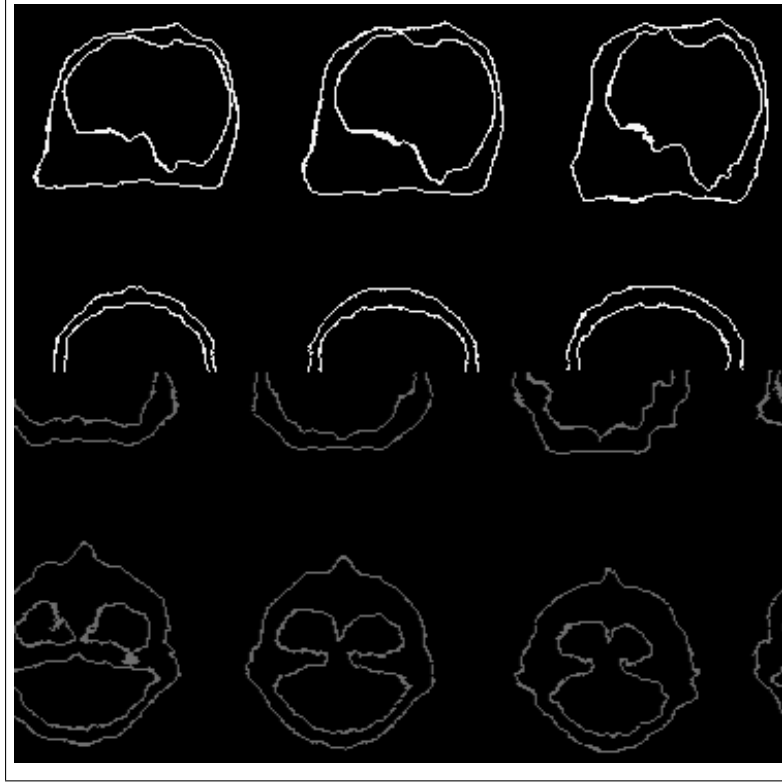
$$\bar{\mathbf{a}} = \begin{pmatrix} \bar{\mathbf{a}}_H \\ \bar{\mathbf{a}}_B \end{pmatrix} \quad (30)$$

In equation (29), the columns of the $3NN' \times 3M'$ matrix Φ_H are the eigenvectors of the spherical mesh describing the head surface and the columns of the $3NN' \times 3M''$ matrix Φ_B are the eigenvectors of the spherical mesh describing the brain surface. Besides, the $3M' \times m$ matrix \mathbf{P}_{HB} and the $3M'' \times m$ matrix \mathbf{P}_{BH} describe the statistical dependences of head and brain vibration amplitudes observed in the training set. Vectors $\bar{\mathbf{a}}_H$ and $\bar{\mathbf{a}}_B$ are of order $3M' \times 1$ and $3M'' \times 1$ respectively, and vector \mathbf{b} has a low dimension $m \ll 3(M' + M'')$. In our preliminary implementation, typical values are $NN' \simeq 20000$, $M' \simeq M'' \simeq \frac{NN'}{4} \simeq 5000$ and $m \simeq 10$. As it can be seen, thanks to the KL representation, only a few parameters ($m \simeq 10$) are necessary to describe the variations of the deformable model.

4. DEFORMABLE MODEL-BASED REGISTRATION

Registration of the multimodal image pair consists in estimating the rigid transformation parameters \mathcal{S}_{rig} (3D rotation and translation parameters) that have to be applied to the image to be registered (here the SPECT image) in order to match the reference image (here the MRI). The registration relies on (noisy) head contours extracted from the MRI and (noisy) brain contours extracted from the SPECT image. These structures do not overlap but the deformable model represents the relative location of the head and brain contours and accounts for the anatomical variability observed among the training population. The deformable model is used as a probabilistic atlas that constrains the rigid registration of the image pair. The transformations between the deformable model and the image pair include the deformation parameter vector \mathbf{b} (representing anatomical variability) and a rigid transformation \mathcal{S}_{mod} .

The rigid and deformable transformation parameters \mathcal{S}_{rig} , \mathcal{S}_{mod} and \mathbf{b} yielding the overall “best” match of the deformable multimodel with the head contour in the MR image and the registered brain contour in the SPECT



$$\mathbf{b}[1] = -\sqrt{\lambda_1}$$

$$\mathbf{b}[1] = 0$$

$$\mathbf{b}[1] = \sqrt{\lambda_1}$$

Figure 3. Deformations of a 3D multimodel by varying the first statistical mode in vector \mathbf{b} between $-\sqrt{\lambda_1}$ and $\sqrt{\lambda_1}$. λ_1 designates the first eigenvalue of the covariance matrix $\mathbf{\Gamma}$. Each column shows a multiplanar (sagittal, coronal, transversal) view of the 3D model.

image are estimated by minimizing a global energy function based on a distance between the model and the contours extracted from the image pair³¹:

$$(\mathcal{S}_{rig}^*, \mathcal{S}_{mod}^*, \mathbf{b}^*) = \arg \min_{\mathcal{S}_{rig}, \mathcal{S}_{mod}, \mathbf{b}} [E(\mathcal{S}_{rig}, \mathcal{S}_{mod}, \mathbf{b})] \quad (31)$$

where:

$$E(\mathcal{S}_{rig}^*, \mathcal{S}_{mod}^*, \mathbf{b}^*) = E_{MR}[\mathbf{X}_H(\mathcal{S}_{mod}, \mathbf{b})] + E_{SPECT}[\mathbf{X}_B(\mathcal{S}_{rig}, \mathcal{S}_{mod}, \mathbf{b})]. \quad (32)$$

E_{MR} is an energy function computed only for the points of $\mathbf{X}_{H,B}$ modeling the head and E_{SPECT} depends only on the points of $\mathbf{X}_{H,B}$ modeling the brain :

$$\begin{aligned} E_{MR}[\mathbf{X}_H(\mathcal{S}_{mod}, \mathbf{b})] &= \sum_{p \in \mathbf{X}_H(\mathcal{S}_{mod}, \mathbf{b})} \Delta_{MR}(p) \\ E_{SPECT}[\mathbf{X}_B(\mathcal{S}_{rig}, \mathcal{S}_{mod}, \mathbf{b})] &= \sum_{p \in \mathbf{X}_B(\mathcal{S}_{rig}, \mathcal{S}_{mod}, \mathbf{b})} \Delta_{SPECT}(p). \end{aligned}$$

In the above equation, $\Delta_{MR}(p)$ and $\Delta_{SPECT}(p)$ designate the chamfer distance between point p of the deformable model and the nearest contour point in the MR and SPECT image respectively³¹ (contours are extracted using simple thresholding techniques²⁶).

The global minimization (31) may be performed by using a stochastic method, alternately minimizing the objective function E with respect to the different transformation parameters $(\mathcal{S}_{rig}, \mathcal{S}_{mod}, \mathbf{b})$.⁷ In practice, for the application considered here, we have resorted to the following suboptimal (but fast) estimation technique :

- Initialize the template by the average model $\mathbf{X}(\mathbf{b} = \mathbf{0})$.
- Do until convergence:
 - Estimate \mathcal{S}_{mod} using a principal axes registration technique, bringing into alignment the deformable model and the MRI.
 - Deform the average model by iteratively computing the components of \mathbf{b} minimizing (32).
- Estimate \mathcal{S}_{rig} using a principal axes registration technique, by bringing into alignment the SPECT image with the deformable model.

Figures 4 and 5 illustrate an example of a MRI/SPECT registration using the proposed technique. As can be seen, although the MRI and SPECT head and brain contours do not overlap, the two images have been correctly registered. *It was also not necessary to remove non brain structures (skull and scalp) before registration.* The images in figure 4(a-b) show the two volumes before and after registration. The different steps of the procedure are presented in figure 5: registration of the average model with respect to the MRI (5(a)), deformation of the head part of the average model with regard to the MRI contours (fig. 5(b)) and matching of the SPECT volume to the deformed part of the model describing the brain (fig. 5(c)). The whole registration procedure takes about 20 min cpu time on a HP C200 workstation for a 128^3 image volume.

5. BRAIN SEGMENTATION

In order to extract the brain structure from a patient MRI volume not belonging to the training set, we first represent its head contour (that has been easily extracted by simple thresholding) by the amplitudes of the vibration modes of $\bar{\mathbf{X}}_H$. The head contour coordinates are then stacked in a vector \mathbf{X}_H . We solve equation (28) in the reduced space corresponding to the head coordinates only, to obtain a first least-squares estimate for vector \mathbf{b} that matches the observed head contour:

$$\mathbf{b} = [(\Phi_H \mathbf{P}_{HB})^T \Phi_H \mathbf{P}_{HB}]^{-1} (\Phi_H \mathbf{P}_{HB})^T (\mathbf{X}_H - \bar{\mathbf{X}}_H - \Phi_H \bar{\mathbf{a}}_H). \quad (33)$$

Let us notice that the above solution is constrained by the matrix \mathbf{P}_{HB} which relates the brain contour to the head contour coordinates, as learned from the training set. Equation (33) provides thus also a *good initial estimation of the location of the brain contour*.

Further improvement of this initial solution may be obtained by alternately optimizing an energy function parameterized by the m components of vector \mathbf{b} ,³ in order to fit the part of the model describing the brain to a noisy contour map I_c extracted from the image.³² In our case, the cost function E to be optimized is defined as:

$$E = \sum_{p \in \mathbf{X}_B(\mathbf{b})|i=1} I_c(p) \quad (34)$$

The above cost function simply counts the number of points of the model located on a contour point of the brain.

To summarize, the overall segmentation algorithm is based on the following steps:

- Computation of the statistical deformation parameters \mathbf{b} by solving the overconstrained system (33).
- Prediction of the brain surface by equation (28).
- Fine-tuning of the solution by deterministic optimization of cost function (34).

Figure 6 presents an example of brain segmentation from 3D MRI. The image in figure 6(a) is a post-operative MRI. In figure 6(b) the head surface is segmented and parameterized by the physics-based deformable model. The head surface coordinates combined with the probabilistic model provides a good prediction of the brain surface (fig. 6(c)) which is then fine-tuned (fig. 6(d)-(e)). The whole segmentation process takes about 10 min cpu time on a HP C200 workstation for a 128^3 image volume.

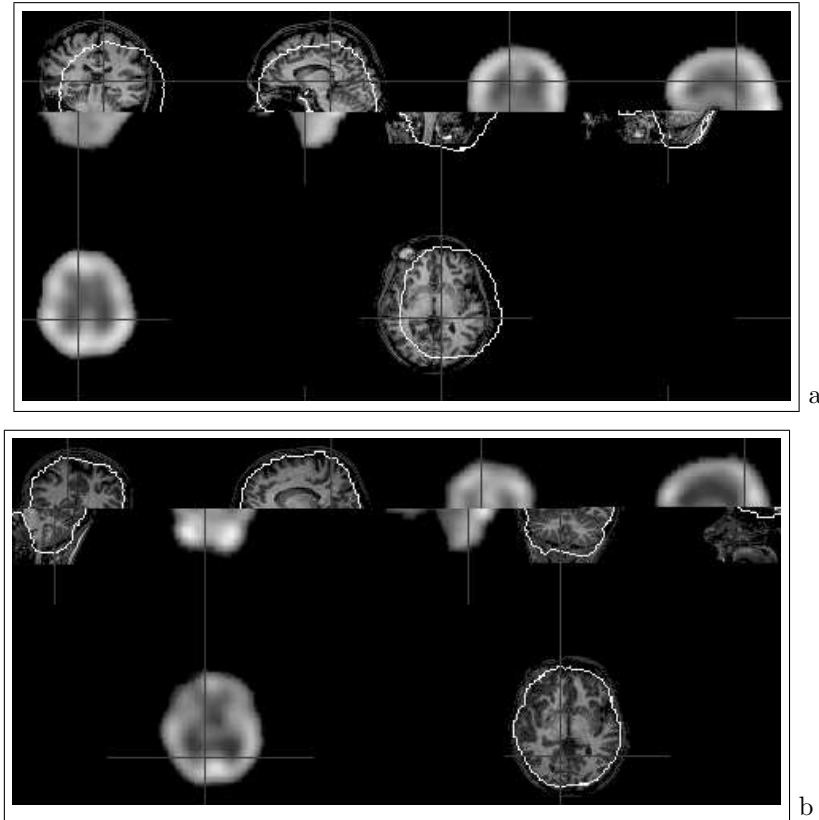


Figure 4. MRI/SPECT registration using the deformable multimodel. (a) MRI and SPECT volumes before (a) and after (b) registration. The SPECT contours are superimposed onto the MRI. The intermediate steps of the registration procedure are shown in figure 5

6. DISCUSSION AND CONCLUSION

We have presented a probabilistic deformable model carrying information both on the spatial relation between head and brain structures and on the anatomical variability of these two structures observed over a representative population. Applications of the probabilistic model include the registration of multimodal image pairs (MRI/SPECT) and the segmentations of anatomical structures from a given modality (MRI).

The major advantage of the technique is that it is based on *a priori* statistical knowledge rather than grey-level information and consequently it is not affected by noise, missing data or outliers. Thanks to the statistical constraints embedded in the deformable model, the method could be applied to the segmentation of the brain structure from post operative images where missing anatomical structures lead standard voxel-based techniques to erroneous segmentations.

The major perspective of our work is to incrementally extend the model by representing other anatomical structures of the brain (ventricles, corpus callosum, hippocampus, etc.) in order to create probabilistic anatomical atlas of the brain.

Acknowledgments

This study has been supported by the Commission of the European Communities, DG XII, in the framework of the TMR program (Training and Mobility of Researchers), contract No ERBFMIBCT960701 and by the “Groupement d’Intrt Scientifique-Sciences de la Cognition” (CNRS, CEA, INRIA, MENESR).

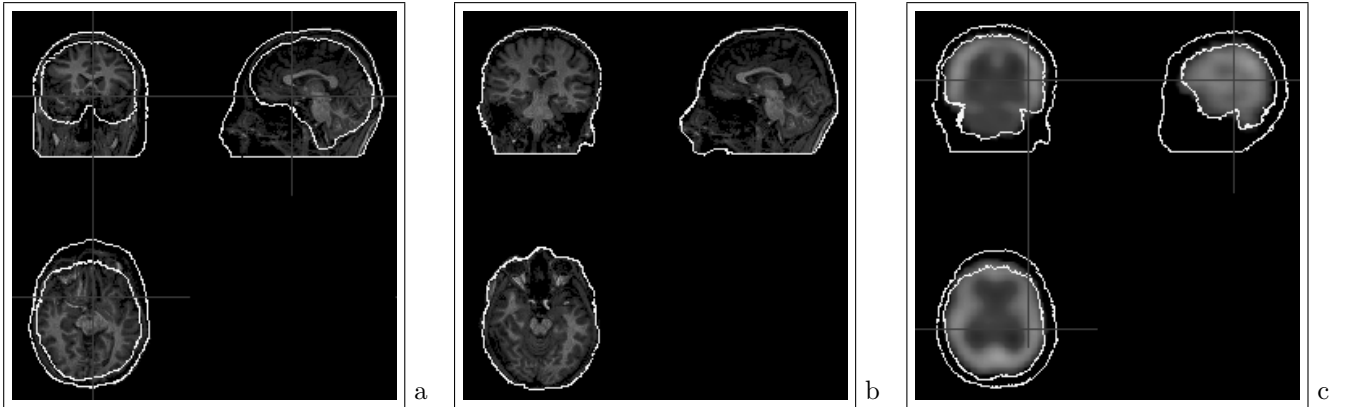


Figure 5. MRI/SPECT registration of the images in figure 4 using the deformable multimodel. (a) Registration of the part of the average model describing the head structure to the MRI. The same rigid transformation parameters are applied to the part of the model describing the brain. (b) Deformation of the part of the average model describing the head structure to the MRI head surface. The same deformation parameters are applied to the part of the model describing the brain. (c) Registration of the SPECT volume to the part of the deformable model describing the brain.

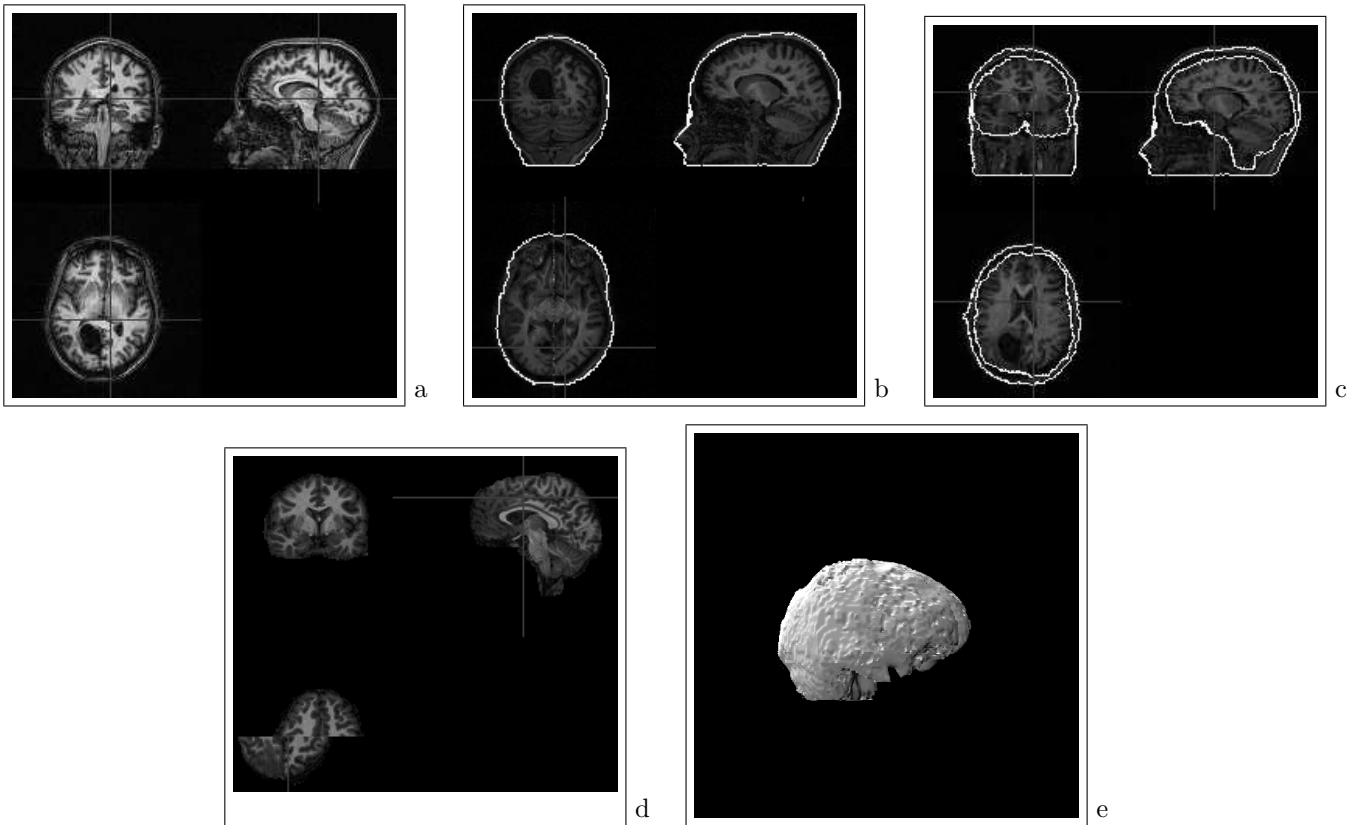


Figure 6. (a) A patient's MR image. (b) Head surface extraction and parameterization of the image in (a). (c) Brain surface prediction using the head surface in (b) and the probabilistic deformable model. (d) The segmented brain in multiplanar view. (e) The segmented brain in 3D view.

REFERENCES

1. M. Kass, A. Witkin, and D. Terzopoulos, "Snakes: active contour models," *International Journal of Computer Vision* **4**(1), pp. 321–331, 1988.
2. T. F. Cootes, C. J. Taylor, and J. Graham, "Active shape models - their training and application," *Computer Vision and Image Understanding* **1**(1), pp. 38–59, 1995.
3. C. Kervrann and F. Heitz, "A hierarchical Markov modeling approach for the segmentation and tracking of deformable shapes," *Graphical Models and Image Processing* **60**(3), pp. 173–195, 1998.
4. C. Nastar and N. Ayache, "Frequency-based nonrigid motion analysis," *IEEE Transactions on Pattern Analysis and Machine Intelligence* **18**(11), pp. 1069–1079, 1996.
5. R. Bajcsy and S. Kovačič, "Multiresolution elastic matching," *Computer Vision, Graphics and Image Processing* **46**, pp. 1–21, 1989.
6. C. Davatzikos, "Spatial transformation and registration of brain images using elastically deformable models," *Computer Vision and Image Understanding* **66**(2), pp. 207–222, 1997.
7. C. Kervrann and F. Heitz, "Statistical model-based segmentation of deformable motion.," in *Proceedings of the 3rd IEEE International Conference on Image Processing (ICIP '96)*, pp. 937–940, (Lausanne, Switzerland), 1996.
8. T. Mc Inerney and D. Terzopoulos, "Deformable models in medical image analysis: a survey," *Medical Image Analysis* **2**(1), pp. 91–108, 1996.
9. U. Grenader and M. I. Miller, "Representation of knowledge in complex systems," *Journal of the Royal Statistical Society* **56**(3), p. 1994, 1994.
10. C. L. Huang, W. T. Chang, L. C. Wu, and J. K. Wang, "Three-dimensional PET emission scan registration and transmission scan synthesis," *IEEE Transactions on Medical Imaging* **16**(5), pp. 542–561, 1997.
11. A. Pentland and S. Sclaroff, "Closed-form solutions for physically-based shape modeling and recognition," *IEEE Transactions on Pattern Analysis and Machine Intelligence* **13**(7), pp. 730–742, 1991.
12. A. Pentland and B. Horowitz, "Recovery of non-rigid motion and structure," *IEEE Transactions on Pattern Analysis and Machine Intelligence* **13**(7), pp. 715–729, 1991.
13. S. Sclaroff and A. Pentland, "Modal matching for correspondance and recognition," *IEEE Transactions on Pattern Analysis and Machine Intelligence* **17**(6), pp. 545–561, 1995.
14. C. Nastar, B. Moghaddam, and A. Pentland, "Flexible images: matching and recognition using learned deformations," *Computer Vision and Image Understanding* **65**(2), pp. 179–191, 1997.
15. P. Thompson, D. MacDonald, M. Mega, C. Holmes, A. Evans, and A. Toga, "Detection and mapping of abnormal brain structure with a probabilistic atlas of cortical surfaces," *Journal of Computer Assisted Tomography* **21**, pp. 567–581, 1997.
16. J. Martin, A. Pentland, S. Sclaroff, and R. Kikinis, "Characterization of neuropathological shape deformations," *IEEE Transactions on Pattern Analysis and Machine Intelligence* **20**(2), pp. 97–112, 1998.
17. L. G. Brown, "A survey of image registration techniques," *ACM Computing Surveys* **24**(4), pp. 325–376, 1992.
18. J. B. A. Maintz and M. A. Viergever, "A survey of medical image registration techniques," *Medical Image Analysis* **2**(1), pp. 1–36, 1998.
19. C. Davatzikos, "Spatial normalization of 3D brain images using deformable models," *Journal of Computer Assisted Tomography* **20**(4), pp. 656–665, 1996.
20. J. Gee, M. Reivich, and R. Bajcsy, "Elastically deforming 3D atlas to match anatomical brain images," *Journal of Computer Assisted Tomography* **17**(2), pp. 225–236, 1993.
21. J. C. Gee, L. LeBriquer, C. Barillot, D. R. Haynor, and R. Bajcsy, "Bayesian approach to the brain image matching problem," in *SPIE Proceedings of the International Conference on Medical Imaging*, vol. 2434, pp. 145–156, 1995.
22. G. Christensen, S. C. Joshi, and M. Miller, "Volumetric transformation of brain anatomy," *IEEE Transactions on Medical Imaging* **16**(6), pp. 864–877, 1997.
23. J. P. Thirion, "Fast intensity-based non-rigid matching," in *Proceedings of the International Conference on Medical Robotics and Computer Assisted Surgery*, pp. 47–54, (Wiley, New York), 1995.
24. J. P. Thirion, "New feature points based on geometric invariants for 3D image registration," *International Journal of Computer Vision* **18**, pp. 121–137, 1996.

25. C. Nikou, F. Heitz, and J. P. Armspach, "Robust registration of dissimilar single and multimodal images," in *Lecture Notes in Computer Science. Proceedings of the 5th European Conference on Computer Vision (ECCV'98)*, Springer-Verlag, ed., vol. 2, pp. 51–65, (Freiburg, Germany), 2-6 June 1998.
26. C. Nikou, J. P. Armspach, F. Heitz, I. Namer, and D. Grucker, "MR/MR and MR/SPECT registration of brain images by fast stochastic optimization of robust voxel similarity measures," *Neuroimage* **8**(6), pp. 30–43, 1998.
27. N. Otsu, "A threshold selection method from grey-level histograms," *IEEE Transactions on Systems, Man and Cybernetics* **9**(1), pp. 62–66, 1979.
28. O. Musse, J. P. Armspach, I. J. Namer, F. Heitz, F. Hennel, and D. Grucker, "Data-driven curvilinear reconstruction of 3D MRI: application to cryptogenic extratemporal epilepsy," *Magnetic Resonance Imaging* **16**(10), pp. 1227–1235, 1998.
29. G. Borgefors, "Hierarchical chamfer matching: a parametric edge matching algorithm," *IEEE Transactions on Pattern Analysis and Machine Intelligence* **10**(6), pp. 849–865, 1988.
30. K. J. Bathe, *Finite element procedures*, Prentice Hall, Englewood Cliffs, New Jersey, 1996.
31. G. Borgefors, "On digital distance transforms in three dimensions," *Computer Vision and Image Understanding* **64**(3), pp. 368–376, 1996.
32. O. Monga and R. Deriche, "3D edge detection using recursive filtering," *Computer Vision and Image Understanding* **53**(1), pp. 76–87, 1991.